Reproducible radiation-damage processes in proteins irradiated by intense x-ray pulses

Stefan P. Hau-Riege and Brian J. Bennion

Phys. Rev. E **91**, 022705 — Published 9 February 2015

DOI: 10.1103/PhysRevE.91.022705

Reproducible radiation damage processes in proteins irradiated by intense x-ray pulses

Stefan P. Hau-Riege and Brian J. Bennion

Lawrence Livermore National Laboratory, Livermore, CA 94550

Abstract. X-ray free-electron lasers (XFEL) have enabled femtosecond protein nanocrystallography, a novel method to determine the structure of proteins. It allows time-resolved imaging of nanocrystals that are too small for conventional crystallography. The short pulse duration helps in overcoming the detrimental effects of radiation damage because x-rays are scattered before the sample has been significantly altered. It has been suggested that, fortuitously, the diffraction process self-terminates abruptly once radiation damage destroys the crystalline order. Our calculations show that high-intensity x-ray pulses indeed trigger a cascade of damage processes in ferredoxin nanocrystals, a particular metalloprotein of interest. However, we found that the damage process is initially not completely random but correlations exist among the protein monomers, so that Bragg diffraction still occurs in the damaged nanocrystals, despite significant atomic displacements. Our results show that the damage process is reproducible to a certain degree, which is potentially beneficial for the orientation step in single-molecule imaging.

Introduction

Nearly a decade before the first hard X-ray free-electron laser (XFEL) became available in 2009 [1], it had been suggested that XFELs could revolutionize biological imaging by enabling atomic-resolution structure determination of single molecules [2]. The concept underlying this innovation is that XFEL pulses are so short in duration that the sample diffracts before it vaporizes [3]. Even though significant progress has been made in this area, including the lower-resolution imaging of single viruses [4], atomic-resolution imaging of single molecules remains a grand challenge.

An important intermediate step was the invention of femtosecond x-ray nanocrystallography [5]. Using protein nanocrystals, it allows atomic-resolution molecular structure determination of proteins that are difficult or impossible to grow into crystals large enough to perform conventional protein crystallography at synchrotrons. Compared to single molecule imaging, this new method features relaxed radiation-dose requirements because high intensity Bragg peaks produce strong signals even for lower incoming x-ray fluences. Since the x-ray pulse destroys the nanocrystal, a new crystal is needed for every shot. This gave rise to the method of serial femtosecond crystallography (SFX), requiring tens of thousands of crystals for every protein structure. Important initial SFX work includes pump-probe experiments on the photosystem I and II complexes [6, 7].

It has been suggested that the rapid loss of the crystalline periodicity induced by radiation damage leads to an abrupt termination of the Bragg diffraction once damage manifests itself. If correct, this concept would significantly help in reducing the effect of damage in nanocrystals on

diffraction because the Bragg peaks would disappear before damage through atomic motion occurs. The method was proposed based on experimental results along with calculations performed using a continuum model for the radiation-matter interaction processes. Naturally, such continuum models neglect certain atomistic details. For example, atomic displacements are added *a posteriori* by assuming random diffusive thermal atomic motion parametrized by the ion temperature [8]. Other experiments suggest that this behavior is actually significantly more complex due to local damage to the structure [9].

The situation becomes more complicated when heavier atoms with a higher atomic number A are present in the molecule. The photoabsorption cross section depends superlinearly on A, and, as a result, these atoms absorb x-rays very efficiently. Enhanced damage near these high-Z hot spots in single molecules has been discussed in the context of pair correlation functions [10]. Recent experiment on the iron-sulfur protein ferredoxin showed indications for preferential damage near and at high-Z elements [11]. In the current study, we used a massively-parallel molecular dynamics (MD) code to explore atomic motion in ferredoxin microcrystals. Each ferredoxin monomer contains two [4Fe-4S] clusters, which are potential localized damage hot spots. In agreement with Reference [10], we found strong atomic displacements near these clusters. However, these displacements are not random, as previously assumed [3, 12], but are reproducible and strongly correlated throughout the crystal. Therefore, atomic motion might not lead to abrupt Bragg peak shutoff through atomic motion at medium resolution but to distinct changes in the individual Bragg intensities during the pulse. Therefore, a continuum model is not appropriate to describe this behavior, especially for protein nanocrystals containing high-Z elements.

Description of the model

We simulated the evolution of the nanocrystals under x-ray irradiation using a version of the massively-parallel MD code *ddcMD* which can efficiently track millions of particles for millions of time steps when executed on large computer systems [13, 14]. *ddcMD* is the centerpiece of Lawrence Livermore's Cimarron Project and has been used in multiple comprehensive studies of high energy density plasma phenomena [14-20]. It utilizes a velocity Verlet integration with a particle-centric domain decomposition method. Long-range Coulomb forces were calculated by the particle-particle– particle-mesh (P3M) method. We have extended *ddcMD* to include the relevant quantum-atomistic processes using the "small ball" approach, and we carefully verified that its predictions match the experimentally-validated atomic kinetics code *Cretin* [17, 21]. Given that the protein nanocrystals are essentially transparent to x-ray radiation, we modeled the photon beam as a uniform photon bath that induces random photoionization events according to the ionization states of the ions. *ddcMD* includes dense-plasma phenomena like continuum lowering in the Steward-Pyatt model [22] and three-body recombination. Since classical electron-ion plasmas rapidly collapse, it is common to modify the Coulomb potential at small particle distances. The quantum mechanical rationale for this modification is the replacement of point particles with de Broglie waves whose scattering exhibits diffractive behavior [23]. We used the commonly-used Dunn-Broyles quantum-statistical potentials (QSP) to account for this phenomenon. Pauli exclusion also modifies the Coulomb interaction between electron pairs, and it too can be mimicked by a statistical potential such as the spin-averaged result of Deutsch [24]. The specific choice of QSP does not affect our results significantly since atomic motion is driven

primarily by the time-averaged (slow) microfields, which we have shown to be potential independent [23]. Instead of simulation the full nanocrystal, we simulate a subvolume and assume periodic boundary conditions. The nanocrystals are sufficiently large that edge and finite size effects, such as Coulomb charging, are negligible. Further, even though the XFEL emits x-ray pulses with a more complex temporal intensity structure, our simulations have shown that a pulse with constant temporal intensity predicts similar evolution dynamics. The simulations were performed in the microcanonical ensemble. Initially, the atoms were assigned random velocities that were consistent with a Maxwellian velocity distribution at room temperature. The time integration was performed with a time step of less than 2×10^{-5} fs which allows us to resolve the fast dynamics of the photoelectrons.

In this work, we considered the ferredoxin protein from the bacterium *Clostridium acidurici*, a metalloprotein for which a recent XFEL experiment performed at the Linac Coherent Light Source (LCLS) has shown distinct radiation damage to its two [4Fe-4S] clusters [11]. A sketch of the ferredoxin protein is shown in Figure 1 (a). The three-dimensional coordinates for ferredoxin were obtained from the protein data bank (PDB) [26, 27] (PDB code 2FDN). A unit cell was created from the asymmetric unit using the Chimera software package [28] which resulted in a ferredoxin multimer consisting of seven monomers. This unit cell was then replicated. The VMD software package [29] was used to solvate and add Na and Cl ions to balance the charge. The resulting picocrystal consists of 224 ferredoxin monomers and contains a total of 566,000 total atoms, and the total number of particles in the simulation is $2x10^6$ including electrons. Analogous to the LCLS experiment, we simulated the irradiation above and below the Fe K absorption edge at 7.4 and 6.9 keV, respectively. The pulse energy for each of these cases

was 1.4 and 1.6 mJ, respectively. These values are reduced by the beamline transmission of about 50%. The beam area was taken to be $(200\ \text{nm})^2$. Further, we assumed that the pulse intensity is constant in time and that the pulse length is 80 fs.

Results

Figure 2 shows the time evolution of the average ionization Z and its standard deviation σ_Z for the dominant atomic species in the nanocrystal which is irradiated either above or below the iron K absorption edge. As expected, the average ionization increases with time and, for the lighter atoms (C, N, and O), eventually saturates when all electrons are stripped off the atoms. Since the lighter atoms absorb less than one x-ray photon on average during the pulse, see Table I, we conclude that most of the ionization events are collisional. This is different for the heavier Fe and S atoms which absorb six to nine photons on average. Whereas iron atoms are present only in the [4Fe-4S] clusters, more S atoms occur close to the cluster. In Figure 2 we distinguish between these different S atom types, and it can be seen that the degree of ionization is not affected by the high-Z clusters [4Fe-4S], even though they constitute an area of very high local ionization. For all atom types except Fe, the effect of the x-ray energy on the average ionization state is small for the x-ray energies considered in this study.

The [4Fe-4S] clusters have a very interesting displacement dynamics as shown in Figure 1(b) and, in planar projection, in Figure 3. Applying suitable translation and rotation operations, we overlaid all [4Fe-4Se] clusters in the nanocrystal at the beginning of the pulse. These initial positions are indicated by the eight larger symbols plotted in the x-y projections. The smaller symbols indicate the atomic positions at (a) 20 fs, (b) 40 fs, (c) 60 fs, and (d) 80 fs during the

pulse. It can be seen that the distributions of positions broaden which is indicative of a diffusive-type behavior. Our atomistic model shows that there are additional correlated displacements of the S and Fe atoms in the nanocrystal. The diffusion and correlated displacements of the S atoms is much larger than for the Fe atoms since the S atoms are lighter. To quantify the diffusive and correlated contributions to the atomic displacement, we extracted the mean position Δ of each atom in the [4Fe-4S] clusters and its standard deviation σ_Δ as a function of time, as shown in Figure 4. The average is taken over all monomers in the nanocrystal. For a pure diffusive atomic displacement, Δ would be zero, whereas for a completely correlated atomic motion, σ_Δ would vanish. It can be seen from Figure 4 that for the first 8 fs, the diffusive motion dominates since the atoms are just starting to be ionized and being accelerated. Then, for S, the correlated motion dominates for tens of fs until, eventually, the diffusive motion has become so extensive that it is comparable to the correlated motion at around 50 to 60 fs. For Fe, the difference between the atomic displacement and the thermal diffusion is also present earlier on in the pulse but less pronounced. We did not observe significant differences in correlations between the two [4Fe-4S] clusters in the molecule.

Motivated by the dominance of correlated displacements of S and Fe in most of the earlier part of the pulse, we investigated the motion of lighter atoms that are ubiquitous in protein molecules, and we found a similar behavior. Figure 5 shows the correlated displacement Δ and the diffuse displacement σ_Δ as a function of time for carbon, one of the dominant atomic species in proteins by weight. Early in the pulse up to about 12 fs, diffusive motion dominates, but then up to 40 fs correlated motion is prevalent.

Discussion

Our results show that whereas x-ray radiation damage is a stochastic process, it is not completely random with regard to ionization states and atomic displacements. The atoms are rapidly ionized during the pulse, but the ion-to-ion variation of the ionization is not very large as evidenced by its relatively small standard deviation σ_Z shown in Figure 2 (b) and (d). Further, the spatial uniformity of atomic ionization states is not strongly affected by the presence of hot spots in the nanocrystal.

Similarly, the motion is, for a large part, also not random. Whereas significant atomic displacements do occur, in particular around high-Z atoms as discussed in terms of pair correlation functions in Reference [10], this motion is actually correlated and reproducible for a significant fraction of the pulse, as we quantified in Figures 4 and 5. This phenomenon is lost in continuum plasma models that are sometimes used to simulate the damage process since information about the trajectory of individual atoms is not included.

Both non-uniform ionization as well as random, diffusive atomic displacements lead to Bragg spot fading which underlies the concept of Bragg termination once damage occurs [8]. However, uniform ionization and correlated motion, which we found to be dominant for a large part of the pulse duration, lead to only changes in the Bragg spot intensity but not their disappearance, thereby rendering them not correctable [9].

Our simulation results are validated by recent experimental results from SFX experiments on ferredoxin microcrystals at LCLS, which show distinct radiation damage to the [4Fe-4S]

clusters and some indications for sulphur displacements, although some experimental uncertainties remain [11]. Our simulations suggest that both [4Fe-4S] clusters in the protein behave similarly, with the motion initiated by a Coulomb explosion caused by the rapid ionization of S and Fe through photoionization and Auger decay. Due to the smaller mass, S undergoes significant correlated atomic displacement. A similar behavior is observed in the other atomic species.

These results have implications for single-molecule atomic-resolution imaging in that they show that even though atomic displacements will be severe, they might have a significant reproducible component from molecule to molecule for each shot. This might simplify orienting the molecules which are injected in random, unknown orientations. Unfortunately, this also shows that these experiments will image the time-averaged atomic trajectories in the protein for sufficiently short pulses and not the original atomic positions.

Acknowledgements

The authors would like to thank Karol Nass, Ilme Schlichting, and Jon Weisheit for helpful discussions. VMD was developed by the Theoretical and Computational Biophysics Group in the Beckman Institute for Advanced Science and Technology at the University of Illinois at Urbana-Champaign. Unit cell structures were produced using the UCSF Chimera package from the Computer Graphics Laboratory, University of California, San Francisco (supported by NIH P41 RR-01081). This work was performed under the auspices of the U.S. Department of Energy by Lawrence Livermore National Laboratory under Contract DE-AC52-07NA27344.

Author contributions

B.J.B. prepared the molecular model and S.H.-R. performed the explosion dynamics calculations. S.H.-R. analyzed the data. Both B.J.B. and S.H.-R. co-authored the manuscript.

References

[1] P. Emma et al., *Nature Photon*. **4**, 641–647 (2010).

[2] R. Neutze et.al.. *Nature* **406**, 752–757 (2000).

[3] H.N Chapman, C. Caleman, and N. Timneanu, *Phil. Trans. R. Soc. B* **369**, 20130313 (2014).

[4] M.M. Seibert et al., *Nature* **470**, 78–81, (2011).

[5] H.N. Chapman et al., *Nature* **470**, 73–77 (2011).

[6] C. Kupitz et al., *Nature* **513**, 261 – 265 (2014).

[7] J. Kern et al., *Science* **340**, 491 – 495 (2013).

[8] A. Barty *et al., Nature Photon*. **6**, 35**–**40 (2012)

[9] L. Lomb et al., Phys. Rev. **B**, 214111 (2011)

[10] Z. Jurek and G. Faigel, Europhys. Lett. **86**, 68003 (2009).

[11] K. Nass et al., Radiation damage in ferredoxin microcrystals using high intensity X-FEL beams, submitted for publication.

[12] C. Caleman, M. Bergh, H.A. Scott, J.C. Spence, H.N. Chapman, and N. Timneanu, *J. Mod. Opt.* **58**, 1486 – 1497 (2011).

[13] D.F. Richards et al., *Proc. IEEE Conference on High-Performance Computing Networking, Storage and Analysis* 1-12 (2009).

[14] F.R. Graziani et al., *High Energy Density Physics* **8**, 105 (2012).

[15] J.N. Glosli et al., *Phys. Rev E* **78**, 205401 (2008).

[16] R. More, F. Graziani, J. Glosli, and M. Surh, *High Energy Density Physics* **6**, 29 (2010).

[17] S.P. Hau-Riege, J. Weisheit, J.I. Castor, R.A. London, H. Scott, and D.F. Richards, *New J. Phys*. **15**, 015011 (2013).

[18] L.X. Benedict et al., *Phys. Rev. E* **86**, 046406 (2012).

[19] P.E. Grabowski, M.P. Surh, D.F. Richards, F.R. Graziani, and M.S. Murillo, *Phys. Rev. Lett*. **111**, 215002 (2013).

[20] S.P. Hau-Riege, *Phys.Rev. E*. **87**, 053102 (2013).

[21] H.A. Scott, *J. Quant. Spect. Radiat. Transf*. **71**, 689–701 (2001).

[22] J.C. Stewart and K.D. Pyatt, *Astrophys. J.* **144**, 1203 (1966).

[23] T. Dunn and A.A. Broyles, Phys. Rev. 157, 156 (1967).

[24] C. Deutsch, M.M. Gombert and H. Minoo, Phys. Letters A66, 381 (1978); A72, 481 (1979).

[25] S.P. Hau-Riege and J. Weisheit, Electric microfields in dense carbon/hydrogen plasmas. Submitted for publication.

[26] H.M. Berman et al., Nucl. Acids Res. 28, 235-242 (2000).

[27] Z. Dauter, K.S. Wilson, L.C. Sieker, J. Meyer, and J.M. Moulis, Biochem. 36, 16065 (1997).

[28] E.F. Pettersen et al., J. Comput. Chem. 25,1605-1612 (2004).

[29] W. Humphrey, A. Dalke, and K. Schulten, J. Molec. Graphics 14, 33-38 (1996).

Figure Captions

Figure 1: Sketch of the ferredoxin protein (left). The displacement dynamics of the [4S-4Fe] clusters is shown on the right. The iron and sulfur atoms are colored red and yellow, respectively.

Figure 2: Average ionization Z and its standard deviation σ_Z as a function of time t. S_i and Fe_i indicate the sulfur and iron atoms, respectively, in cluster i = 1, 2, and H, C, N, O, S the average ionization in the rest of the molecule and solvent. (a) and (b) for $E_{x\text{-}ray}$ = 7.4 keV, and (c) and (d) $E_{x\text{-}ray}$ = 6.9 keV.

Figure 3: X-y projection of the spatial position of the S and Fe atoms in the [4S-4Fe] cluster 1 for all monomers (shifted and rotated so that the clusters coincide before the pulse begins). The large symbols indicate the initial S and Fe atomic positions. (a) 20 fs, (b) 40 fs, (c) 60 fs, and (d) 80 fs.

Figure 4: Correlated displacement Δ and diffusion length σ_Δ of the S and Fe atoms as a function of time t. (a) Cluster 1 at 7.4 keV, (b) cluster 2 at 7.4 keV, (c) Cluster 1 at 6.9 keV, and (d) cluster 2 at 6.9 keV.

Figure 5: Correlated displacement Δ and diffusion length σ_Δ of the C atoms as a function of time *t*.

Tables

Table I. Average number of photoionization events for the dominant atom types at the end of the pulse for nanocrystals irradiated above and below the Fe K edge.

E_{xray} (keV)	H	C	N	O	S	Fe
7.4	0.0	0.3	0.5	0.9	6.4	7.4
6.9	0.0	0.4	0.7	1.2	6.9	9.2

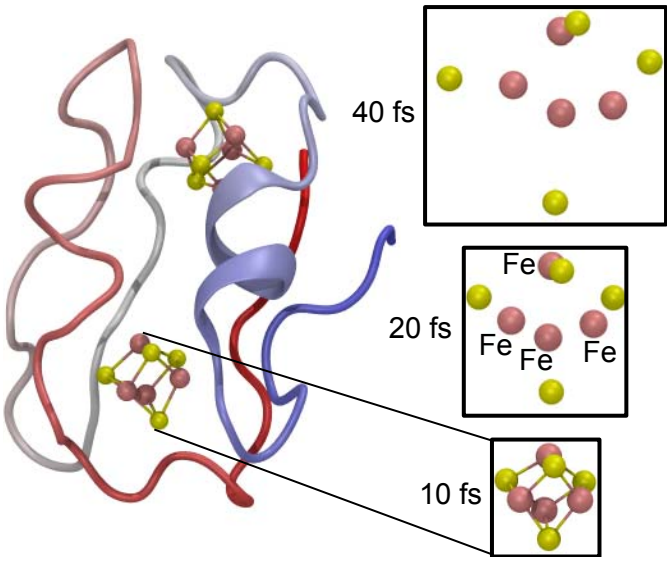

Figure 1

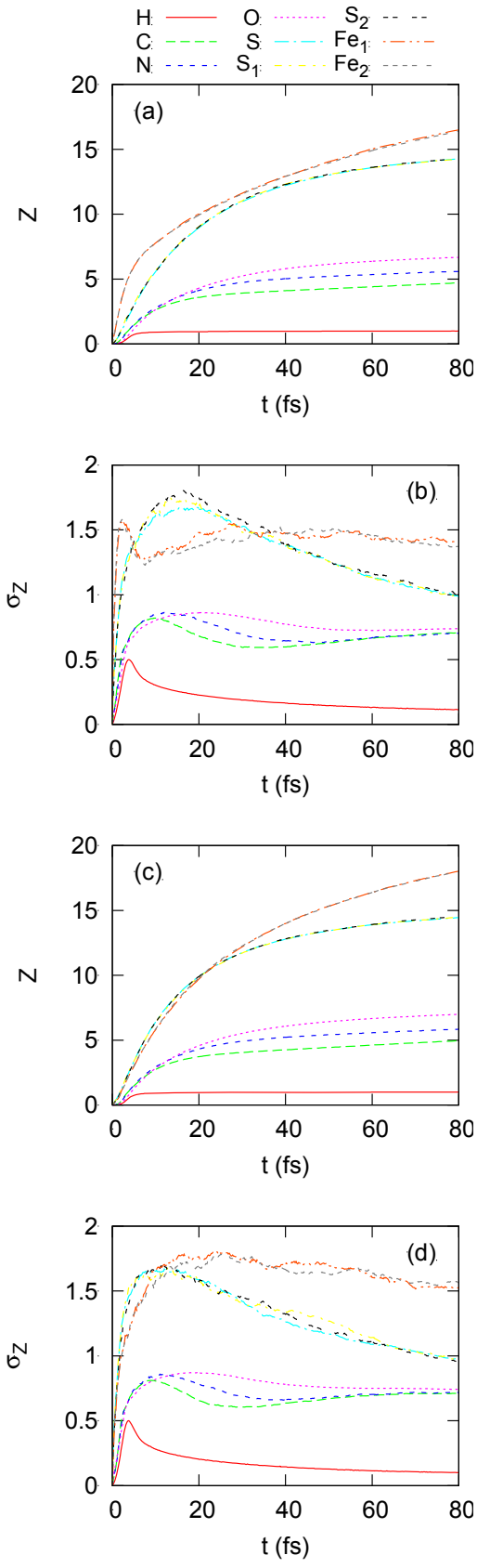

Figure 2

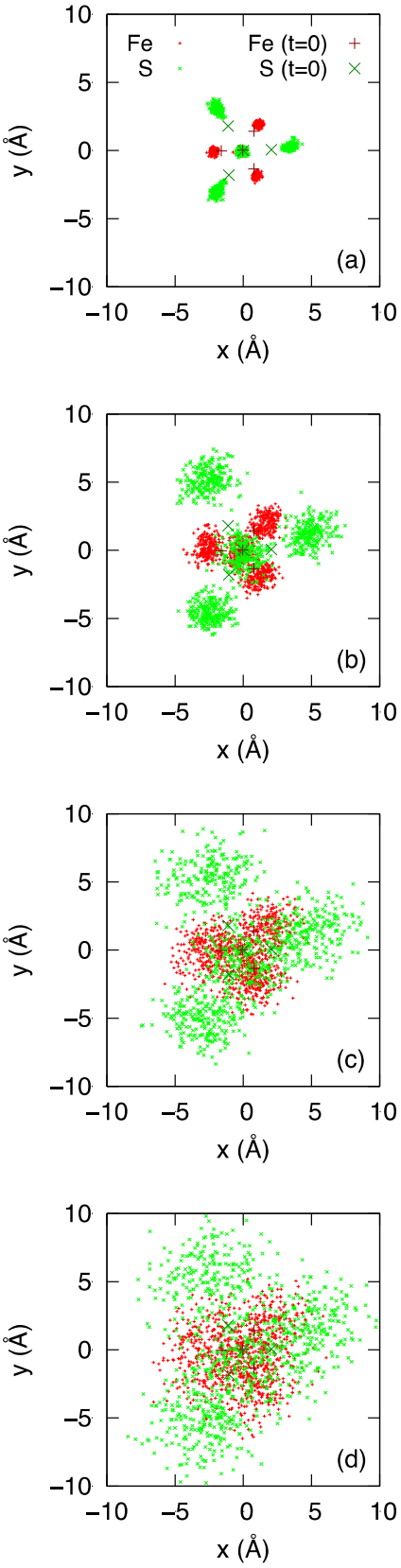

Figure 3

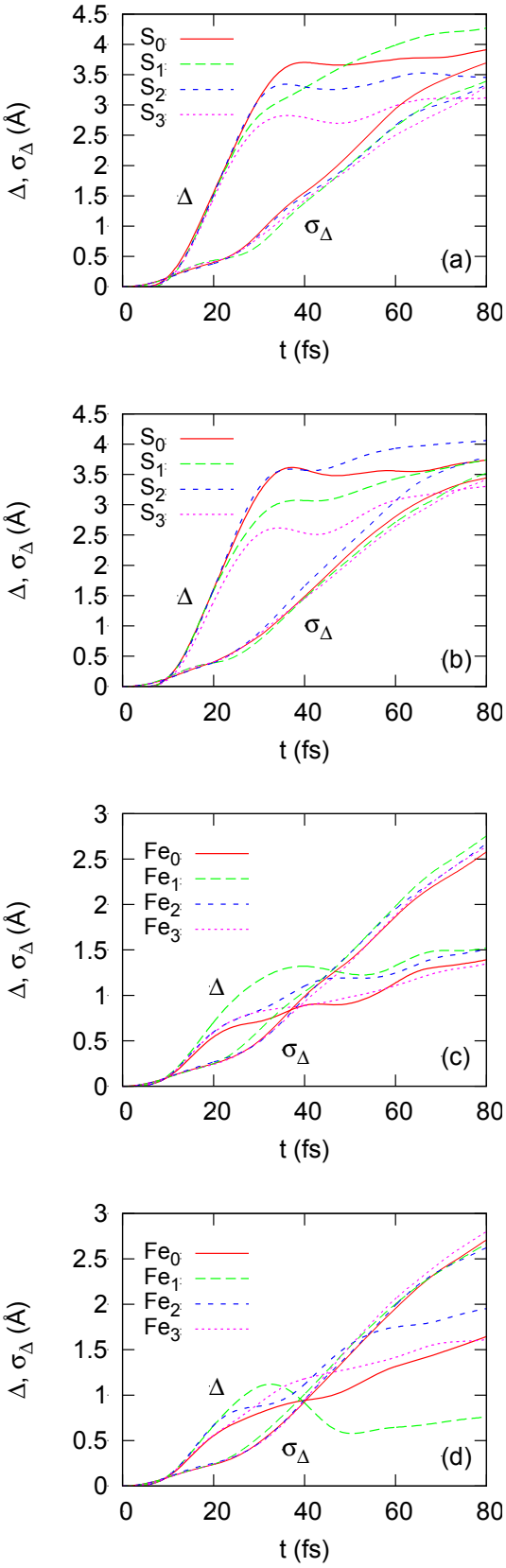

Figure 4

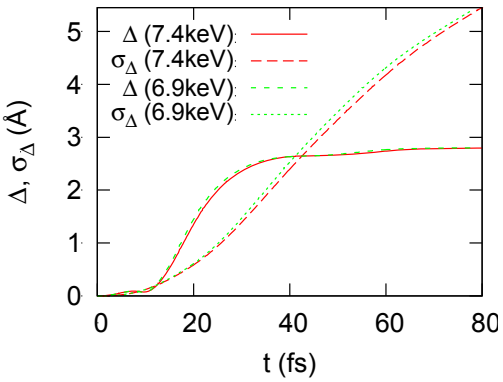

Figure 5